Journal of Zhejiang University-SCIENCE B in press
www.jzus.zju.edu.cn; www.springer.com/journal/11585
E-mail: jzus_b@zju.edu.cn

Research Article
https://doi.org/10.1631/jzus.B2600335

Tmem59 deficiency alters the aging-related transcriptional landscape and neuronal differentiation trajectory in globose basal cells and olfactory sensory neurons

Ping ZHOU[1], Weihao LI[1,2,3], Yiqun YU[1,2,3]✉

[1]*ENT Institute and Department of Otorhinolaryngology, Eye & ENT Hospital, Fudan University, Shanghai, 200031, China*
[2]*Olfactory Disorder Diagnosis and Treatment Center, Eye & ENT Hospital, Fudan University, Shanghai 200031, China*
[3]*Shanghai Key Laboratory of Gene Editing and Cell Therapy for Rare Diseases, Fudan University, Shanghai 200031, China*

Abstract: Neurogenesis in the mammalian olfactory epithelium is a continuous process. Our previous study showed that transmembrane protein 59 (Tmem59) is a critical regulator of epithelial homeostasis, while its deficiency leads to impaired proliferation, loss of sensory neurons, and inflammatory activation; however, the underlying mechanism has not been clarified. In the current study, single-cell RNA-sequencing data were analyzed, revealing that Tmem59 deficiency induces a senescent state in olfactory epithelial cells and the differential expression of aging-related genes as well as genes associated with nasal diseases in basal cells and sensory neurons. The intercellular communications between globose basal cells and sensory neurons were enhanced, while the target genes in sensory neurons were associated with cell growth and differentiation. Along the differentiation trajectory, upregulated genes in Tmem59$^{-/-}$ mOSNs were associated with macroautophagy, such as Ambra1 and Prkn. Tmem59 deficiency was shown to impair cell proliferation and neuronal generation and enhance cell apoptosis in the OE. We also identified several transcriptional network hubs in immune cells, and the target genes to these hubs in Tmem59$^{-/-}$ cells were associated with several critical signaling pathways such as chemokine and Rap1. Finally, Tmem59$^{-/-}$ organoids exhibited a differential expression of genes related with nasal diseases. Collectively, Tmem59 deficiency leads to a series of abnormities at the transcriptional level such as senescent features and an aberrant neuronal differentiation trajectory, potentially putting forward important targets for the treatment of nasal diseases.

Key words: Tmem59; Olfactory epithelium; Basal cell; Olfactory sensory neuron; Macroautophagy

1 Introduction

The olfactory epithelium (OE) mainly consists of basal cells including horizontal basal cells (HBC) and globose basal cell (GBC), immature and mature olfactory sensory neurons (OSN), and sustentacular cells (Schwob et al., 2017). With severe injury, HBCs are rapidly activated to mediate the OE regeneration (Gadye et al., 2017). Under normal physiological conditions, HBCs primarily remain quiescent, while GBCs are responsible for the continuous turnover of olfactory epithelial neurons (Li et al., 2024). This process replenishes naturally dying OSNs, sustaining steady-state renewal (Wu et al., 2025). Based on differential molecular markers, GBCs have been further subdivided into transient amplifying cells (TACs) and immediate neuronal

✉ Yiqun YU, yu_yiqun@fudan.edu.cn
Yiqun YU, https://orcid.org/0000-0001-5256-7082
Ping ZHOU, https://orcid.org/0009-0006-2831-728X
Weihao LI, https://orcid.org/0009-0003-9854-147X

Received May 14, 2026; Revision accepted June 1, 2026;
Crosschecked xxx. xx, 20xx

precursor cells (INPs), playing a crucial role in both self-renewal and the generation of new OSNs (Ko et al., 2023).

Transmembrane protein 59 (Tmem59), also referred to as dendritic cell factor 1 (Dcf1), plays multiple roles in the central nervous system. Tmem59 knockout impairs learning and memory (Liu et al., 2018), while Tmem59 deletion in microglia results in autism-like behavioral deficits (Meng et al., 2022). Tmem59 was also found to modulate inflammation. Tmem59 knockout promotes microglial activation in hippocampal tissue and differentially modulates proinflammatory factors expression (Wang et al., 2018). In ischemic stroke models, Tmem59 expression is downregulated in microglia, while the expression of proinflammatory factors increases, demonstrating that Tmem59 knockout promotes neuroinflammation (Zhang et al., 2021). Our previous research has shown that Tmem59 deficiency results in the loss of OSNs, triggers inflammation in the OE, which in turn disrupts olfactory function, indicating that Tmem59 is essential for OE homeostasis (Ma et al., 2023). However, the molecular mechanisms linking Tmem59 to tissue homeostasis require further investigation.

In this study, single-cell RNA sequencing (scRNA-seq) was conducted on the OE tissues from both wild-type (WT) and Tmem59$^{-/-}$ mice. Our findings indicated massive transcriptomic alteration with Tmem59 deficiency, including higher gene set scores associated with senescence, differential expression of aging- and nasal diseases-related genes, enhanced interactions between GBC and OSN, abnormal neuronal differentiation trajectory with higher expression of autophagy-related genes, and the upregulation of transcriptional hubs in immune cells such as Zeb2 in macrophages. Experimentally, Tmem59 deficiency impaired cell proliferation and neuronal homeostasis and enhanced apoptosis in the OE. Furthermore, Tmem59$^{-/-}$ OE organoids showed a differential expression of genes related with nasal diseases. Collectively, these data exhibit distinct features in the Tmem59$^{-/-}$ OE at the single-cell transcriptional level, providing several potential targets against aging and diseases of the olfactory system.

2 Materials and methods

The methods used in this study for animal experiments, tissue dissection (Wang et al., 2021) and single-cell RNA sequencing, scRNA-Seq raw data processing, quality control and data processing, cell type identification, identification of differentially expressed genes, gene ontology (GO) and pathway enrichment analysis, gene set enrichment analysis (Li, et al., 2024), OE organoid culture (Ren et al., 2021), cryosection preparation and RNA in situ hybridization, immunostaining (Liu et al., 2026), and statistical analysis (Wu, et al., 2025) were described in previous publications, with details provided in the supplementary information.

2.1 Differential abundance testing

Differential abundance (DA) testing was performed using Bioconductor’s miloR (v2.3.1) package. Overlapping cell neighborhoods were defined based on the K-nearest neighbor (KNN) graph. The sampling proportion was set to 0.1, and the refined parameter was set as TRUE. The absolute number of cells from each sample within each neighborhood was quantified using the “countCells” function. Spatial topological distances between neighborhoods were computed using the “calcNhoodDistance” function to allow for multiple hypothesis testing correction. For statistical testing, the WT group was set as the reference baseline, and a negative binomial generalized linear model (GLM) was fitted using the “testNhoods” function to calculate the log-fold change and statistical significance of abundance shifts for each neighborhood in KO mice. For visualization, beeswarm plots were generated using the “plotDAbeeswarm” function to display significant neighborhoods (P-value < 0.05). The arithmetic mean of the overall LogFC shifts was calculated and superimposed as reference lines for each cell type.

2.2 Neighborhood-resolution differentially expressed genes and functional enrichment analysis

On the basis of the DA testing results, target cell neighborhoods exhibiting significant abundance changes

(P-value < 0.05) were extracted. To reduce background noise, low-abundance genes expressed in less than 5% of the total cells were filtered out. A differential expression model comparing KO against WT was independently fitted within each targeted neighborhood using the "de_test_neighbourhoods" function from the MiloDE (v0.1.0) package. Upregulated and downregulated genes were extracted after applying spatial multiple testing correction (parameter was set as pval_corrected_across_nhoods < 0.05), and the number of neighborhoods showing significant changes for each gene was quantified. To obtain high-confidence differentially expressed gene sets, only genes demonstrating significant differential expression in at least 50% of the targeted neighborhoods were retained. These highly confident up- and downregulated gene sets were then subjected to GO functional enrichment analysis using the R package clusterProfiler. Finally, the top-ranked enriched GO terms were visualized using ggplot2 (v3.5.1).

2.3 Marker gene analysis

Using Seurat (v5.3.1), positive marker genes of each cell type were identified via "FindAllMarkers" with thresholds (|log2FC| > 0.2, min.pct = 0.25). The top 300 markers per cell type (ranked by avg_log2FC) were extracted. GO Biological Process (BP) enrichment across all identified cell types was performed with the "enrichCluster" function from the clusterProfiler package (v4.14.6), and visualizations including gene expression line plots, marker gene heatmaps were generated using the ClusterGVis (v0.1.2) and the ComplexHeatmap (v2.22.0) package.

2.4 Pseudotemporal trajectory analysis

To reconstruct the developmental trajectory of OSNs between the Tmem59$^{-/-}$ and the wild-type group, the monocle3 package (v1.3.7) was applied to trajectory analysis. First, we extracted GBC_TA, GBC_INP, iOSN, and mOSN data from the preprocessed Seurat object. A total of 1,000 cells of various types were randomly selected and subjected to the standard preprocessing steps. Batch effect correction was implemented using the Harmony algorithm. CDS was constructed using UMAP coordinates, raw UMI count data and cell metadata derived from the new Seurat object. The constructed trajectory was visualized by the "plot_cells" function. To identify genes whose expression dynamics correlated with pseudotime progression, a test was conducted using the " graph_test " function and genes with Moran's I > 0.01 and q_value < 0.05 were defined as trajectory-associated differential expression analysis (DEGs). Genes with similar expression patterns were grouped into modules using the "find_gene_modules" function. The expression patterns of the identified gene modules were visualized by the "plot_cells" function.

2.5 Transcription factor regulatory network analysis

To assess transcription factor regulatory activity across immune and inflammation-related cells, we employed the GEne network inference with ensemble of trees (GENIE3) pipeline. DEGs in T cells, neutrophils, macrophages and monocytes were extracted, and transcriptional factors (TFs) were filtered out. TFs of mm10 were used as a reference list. The GENIE3 package (v1.24.0) was used to construct a gene regulatory network. To refine the network structure and focus on biologically meaningful regulatory interactions, we filtered the predicted regulatory links by setting a weight threshold of 0.1, retaining only those links with a weight > 0.1 for subsequent network analysis. The resulting gene regulatory network was then visualized using Cytoscape software (v3.10.4).

2.6 Cell-cell communication analysis

We performed cell-cell differential communication analysis using the CellChat R package (v2.1.2). CellChat objects were constructed for the Tmem59$^{-/-}$ and wild-type groups separately using the "RNA" assay data and metadata, and the mouse-specific CellChatDB was assigned as the reference database. Subsequently, the default analysis pipeline of CellChat was followed. CellChat objects of Tmem59$^{-/-}$ and wild-type groups were merged for comparative analysis. Differential cell-cell communications between the two groups were

visualized via interaction count heatmaps. NicheNet analysis was performed to explore ligand-receptor (LR) interactions from GBC to OSN. Human NicheNet databases were first converted to mouse gene symbols. DEGs were identified for both sender (GBC) and receiver (iOSN/mOSN) cells via the "FindMarkers" function in Seurat (v5.3.1). Expressed genes in receiver cells (expression percentage > 0.10) were used as background genes. Predicted interactions derived from the "ppi_prediction_go" and "ppi_prediction databases" were excluded, and only high-confidence ligand-receptor pairs were retained for subsequent analyses following the default analytical pipeline of NicheNet. Ligands were ranked by Pearson's correlation coefficient in a descending order, and the top-ranked ligands were prioritized as key upstream ligands. Heatmaps were generated to visualize ligand activities and ligand-target regulatory networks. The circos plot was generated using the "circlize" package to visualize ligand-receptor interaction networks from GBC to OSNs. A functional enrichment of predicted target genes was executed utilizing clusterProfiler with the org.Mm.eg.db database, focusing on Biological Process (BP) terms ($q < 0.05$). The top GO terms were extracted, and bar plots were generated by ggplot2 (v3.5.1).

2.7 OE organoid bulk RNA-seq analysis

The independent isolation of total mRNA was performed for each of the six organoid replicates, including three wild-type samples and three Tmem59$^{-/-}$ samples. For each genotype, three biological replicates were derived from three separate wells of the same original sample at passage 1 to passage 3. Each sample contained the total cell yield from a single well of a 24-well plate. These RNA samples were prepared and then subjected to strand-specific RNA-seq with a reference genome by OE Biotech Co., Ltd. (Shanghai, China). Sequencing reads were mapped against the target reference genome employing HISAT2, generating genome alignment profiles for each sample with alignment rates ranging from 98.86% to 99.36%. After obtaining read counts from the alignment results, genes with zero counts across all samples were filtered out. Bioinformatic profiling was accomplished by employing the OECloud tools (https://cloud.oebiotech.com/task/).

3 Results

3.1 Research design and scRNA-Seq analysis of the olfactory epithelium

To investigate alterations by Tmem59 deficiency, we dissected OE tissues from three WT and two Tmem59$^{-/-}$ mice and subjected them to scRNA-Seq. The 10 × Genomics Cell Ranger pipeline was used to analyze the sequencing data. We performed filtering to discard potential homotypic doublets (>6000 genes) (Luecken and Theis, 2019). Heterotypic doublets identified by DoubletFinder were excluded. A threshold of at least 1,000 UMIs was applied for cell retention. Genes with expression in a minimum of three cells were carried forward for downstream clustering and cell-type identification (Figs. S1a-S1d). After cell filtering and quality assessment, 57,759 single cells underwent subsequent analysis. Data were embedded into two dimensions using t-distributed stochastic neighbor embedding (tSNE). Using the expression matrix of their specific markers, we classified the cells into 16 distinct types (Fig. 1a). Differential abundance testing revealed increases in GBC, HBC and OEG populations, but decreases in mOSN and Sustentacular cell populations (Fig. 1b). Neighborhood-resolution differential expression analysis via the miloDE algorithm and subsequent functional enrichment revealed that energy derivation by oxidation of organic compounds, mitochondrial respirasome assembly, and translation at synapse were downregulated in Tmem59$^{-/-}$ mOSNs (Fig.S1e). Protein localization to cell periphery, postsynapse organization and developmental cell growth were upregulated in Tmem59$^{-/-}$ GBC (Fig. S1f). By visualizing highly expressed genes in each cell cluster via dot plots, we obtained a comprehensive overview of the annotated cell phenotypes. (Fig. 1c). We used tSNE plots to visualize marker genes of selected cell types (Fig. 1d). Biological processes were identified by GO enrichment analysis performed on the top 20 marker genes per cell type (Fig. 1e). To show the cell composition of individual OE samples from WT and Tmem59$^{-/-}$ mice, tSNE plots were used (Fig. S1g). Therefore, this early investigation of OE from WT and

Tmem59$^{-/-}$ mice indicates that it recapitulates the range of cell populations present in original olfactory epithelial tissues.

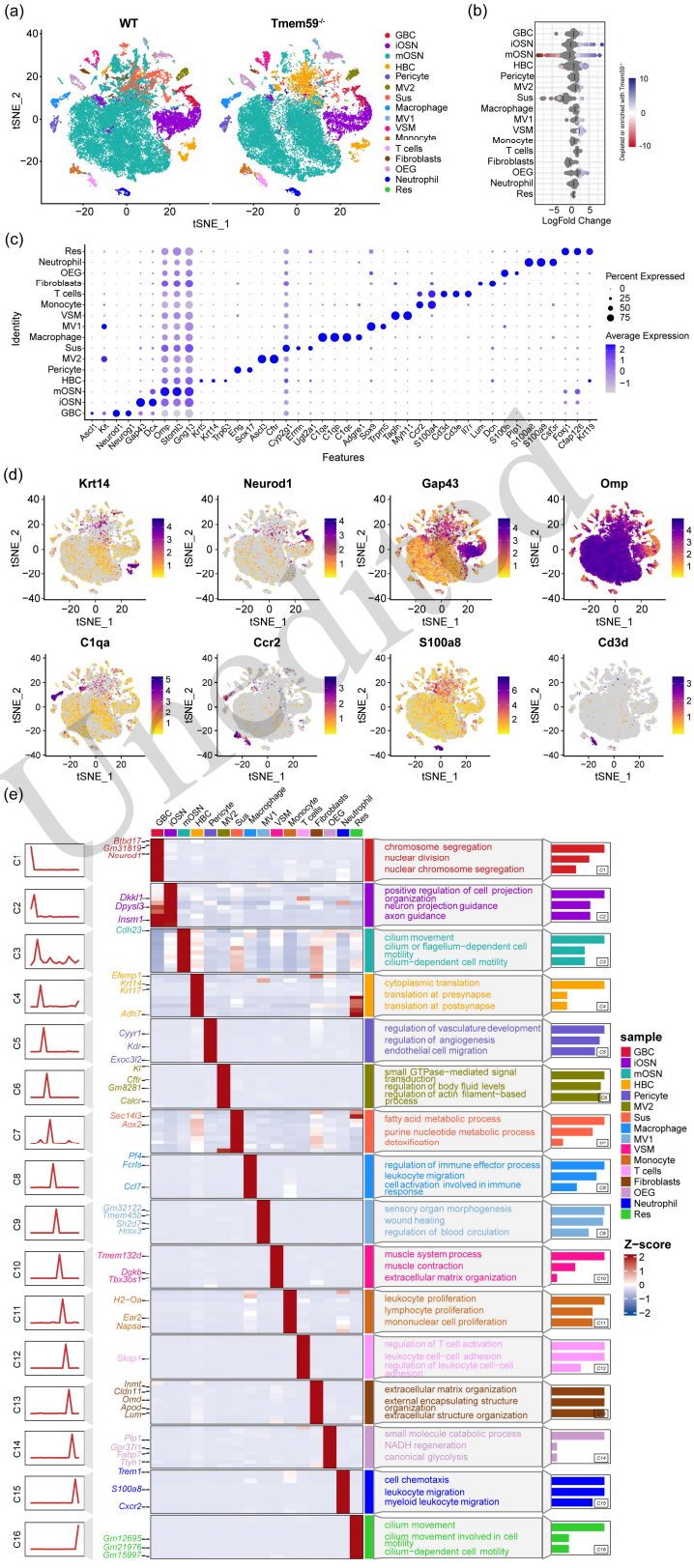

Fig. 1 scRNA-Seq analysis of OE tissues from WT and Tmem59$^{-/-}$ mice. (a) tSNE plot showing the distribution of various OE cell types. (b) Differential abundance testing of Tmem59$^{-/-}$clusters in comparison to WT clusters. (c) Dot plot showing the markers for different cell types. (d) tSNE plots showing marker expression. (e) Heatmap of top markers in each cell type and their respective biological functions by GO term presentation.

3.2 Tmem59 deficiency changes the expression of aging-related genes in GBCs

To determine if Tmem59 knockout causes aging-related changes in the OE, we conducted gene set score analysis to show that the majority of cell types in Tmem59$^{-/-}$ OE exhibited higher scores of cellular senescence and SigRS database (Wang et al., 2025a) compared to their WT counterparts (Figs. 2a and 2b), suggesting that Tmem59 deficiency leads to senescent states in various OE cell types. A significant decrease in 44 ± 7% (P<0.001) in the ratio of Cdkn1a^{+}/ICAM1^{+} HBCs was observed by immunochemical analysis in Tmem59$^{-/-}$ OE compared to WT controls (Figs. 2c and 2d), while the percentage of Cdkn1a^{+}/OMP^{+} mOSNs was increased by 97 ± 20% (P<0.001) in Tmem59$^{-/-}$ OE (Figs. 2e and 2f). tSNE plots showed that Apoe expression was increased in Tmem59$^{-/-}$ OE (Figs. 2g1and 2g2). We then screened DEGs in GBCs using the GenAge database and found 17 upregulated aging-related genes in Tmem59$^{-/-}$ GBCs (Fig.2h). These included Apoe [a critical factor in olfactory information processing (Zhang et al., 2018)], Nfkb1 (a central component for NF-kappaB signaling), Cdc14b (a regulator for cell cycle process, and IGF1R [a suppressor for neurogenesis and olfactory function (Chaker et al., 2015)] (Fig.2H). Those aging-related genes downregulated in Tmem59$^{-/-}$ GBCs included Txn1 that plays anti-inflammatory and neuroprotective roles (Jia et al., 2024), and Cebpb, a hub in transcriptional network of OE aging (Li, et al., 2024) (Fig. 2k). Immunochemical data showed a significant 50 ± 14% (P<0.001) increase in the ratio of Apoe^{+}NeuroD1^{+} GBCs in Tmem59$^{-/-}$ OE versus WT controls (Figs. 2I and 2J), while the percentage of Sox2^{+}Cebpb^{+} GBCs was reduced by 25 ± 10% (P<0.05) in Tmem59$^{-/-}$ OE (Fig. 2l and 2M). These results showed that histological expression differences in aging-related genes between Tmem59$^{-/-}$ and WT GBCs aligned with our scRNA-Seq data. We then subclassified GBCs into transient amplifying cells (TACs) and intermediate neuronal progenitors (INPs) based on their molecular markers (Figs. S2a-S2e). Gene set score analysis showed that INPs in Tmem59$^{-/-}$ OE showed increases in DNA damage response and decreases in stemness, while Tmem59$^{-/-}$ TACs did not exhibit significant differences when compared to the WT counterparts (Fig. S2f). Besides, either Tmem59$^{-/-}$ TACs or INPs showed lower scores of unfolded protein response (UPR) gene set. However, Tmem59$^{-/-}$ TACs or INPs did not show differences in the cell cycle gene set score, compared to WT cells (Fig. S2f). Collectively, we conclude that Tmem59 deficiency leads to the differential expression of aging-related genes in GBCs, potentially affecting DNA damage response, stemness, and unfold protein response.

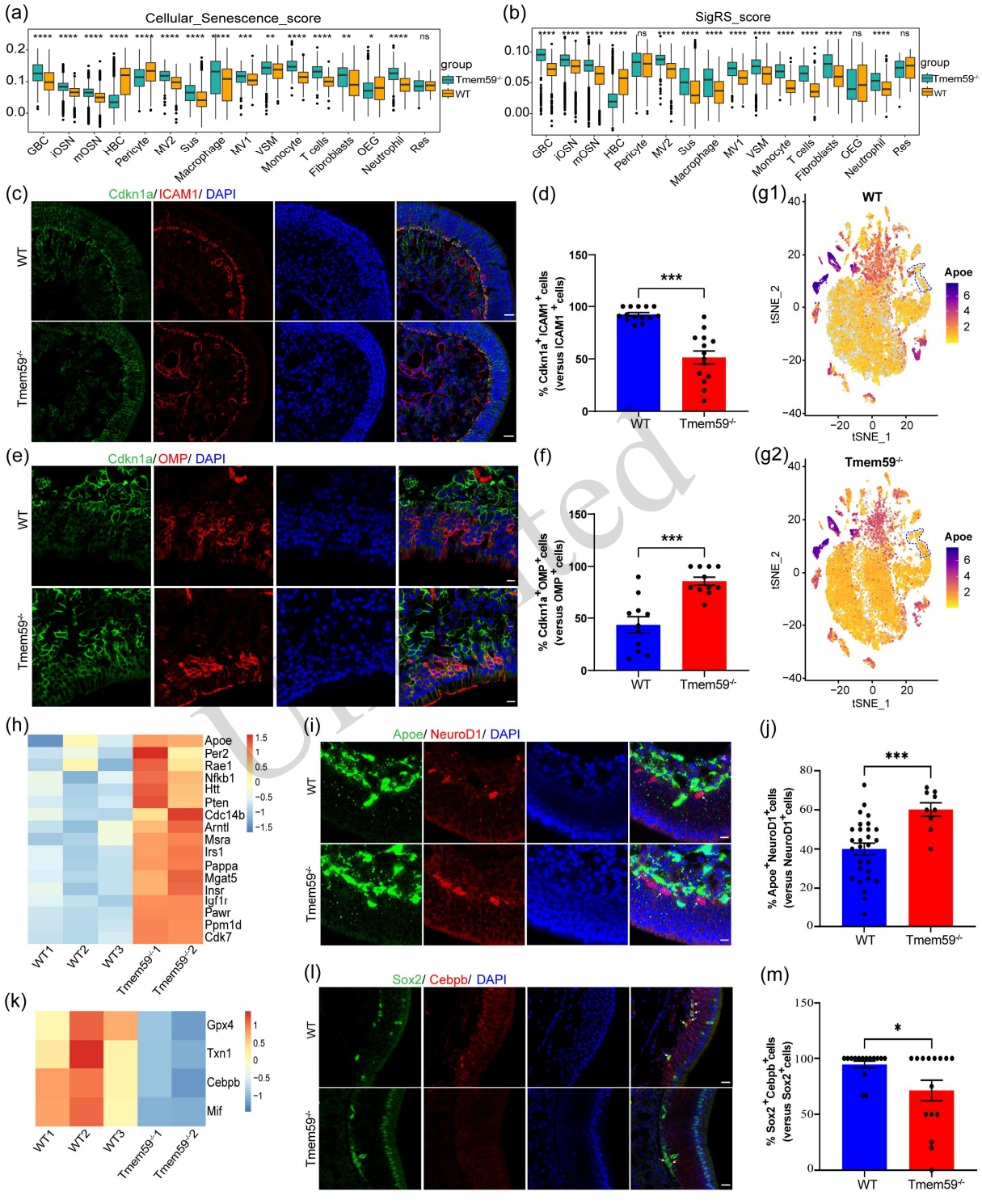

Fig. 2 Tmem59 deficiency leads to senescent state in GBC and other OE cell types. (a, b) Box plots showing gene set score of cellular senescence (a) and aging gene set SigRS (b). (c, e) Confocal images of Cdkn1a^{+} cells in ICAM1^{+} HBCs (c) and Cdkn1a^{+} cells in OMP^{+} mOSN cells (e) from WT and Tmem59$^{-/-}$ OE. (d, f) Quantification of Cdkn1a^{+}ICAM1^{+} (d) and Cdkn1a^{+}OMP^{+} cells (f) in the WT and Tmem59$^{-/-}$ OE. (g) tSNE plots showing Apoe expression. The blue dashed line indicates the distribution of GBCs. (h, k) Heatmaps of common upregulated (h) and downregulated (k) genes in Tmem59$^{-/-}$ GBCs compared to WT counterparts, screened within the GenAge database. (i, l) Confocal images of Apoe^{+} cells in NeuroD1^{+} GBCs (i) and Cebpb^{+} cells in Sox2^{+} basal cells (l) from WT and Tmem59$^{-/-}$ OE. (j, m) Quantification of

Apoe^{+}NeuroD1^{+} (j) and Cebpb^{+}Sox2^{+} cells (m) in the WT and Tmem59$^{-/-}$ OE. The statistical difference was determined by two-tailed Wilcoxon rank-sum test in (a, b), and by unpaired t test in (d, f, j, m). ns, not significant, *p<0.05, **p<0.01, ***p<0.001, ****p<0.0001. All statistical data were from three mice in each group. Scale bars: 25 μm in (c, l), 10 μm in (e, i).

3.3 Tmem59 deficiency promotes intercellular communications from GBCs

We next determined whether Tmem59 regulates intercellular communication between GBCs and other cell types. CellChat analysis showed that the numbers of interactions from GBC to iOSN and mOSN were higher in Tmem59$^{-/-}$ OE than in WT tissue (Figs. 3a-3c). In either Tmem59$^{-/-}$ iOSNs or mOSNs, upregulated Apoe in GBCs bound to Vldlr and Sorl1 (Figs. 3d and 3e), both of which are risk genes for neurodevelopmental disorders and neurodegeneration (Lane-Donovan and Herz, 2017; Lee et al., 2023). Upregulated Semaphorin Sema3a in Tmem59$^{-/-}$ GBCs bound to neuropilin Nrp1 in sensory neurons is reported to be an inhibitory axis for neurite growth of sensory and motor neurons (Shen et al., 2023), while upregulated Sema4d interacts with Plxnb1, functioning in inhibitory synapse development (Mcdermott et al., 2018) (Figs. 3d and 3e). These data suggest that Tmem59 deficiency promotes communication from GBC to sensory neurons and subsequently affects neural activities. Upregulated ligands from GBCs that modulate target genes in iOSNs included cell proliferation genes Ccnd1, Trp53, Bcl2, Brca1, inflammation-related genes IL1β, Bhlhe40, Cxcl5, Ccl7, and Wnt signaling genes Axin2, Lef1, Wnt4 (Fig. 3f), and these targeting genes in iOSNs function in cell differentiation, Wnt signaling pathway, and chemotaxis (Fig. 3h). Similarly, upregulated ligands in GBCs modulate target genes in mOSNs, associated with cell proliferation (Cdkn1a, Trp53, Bcl2, Brca1) and other important transcriptional factors such as Stat3, Zeb2, Lef1 (Fig. 3g). These target genes upregulated in Tmem59$^{-/-}$ mOSNs are associated with hypoxia, response to TGFβ, and negative regulation of cell growth (Fig. 3i). Collectively, Tmem59 may regulate intercellular communication between GBC and OSN, potentially via affecting cell proliferation and cell differentiation.

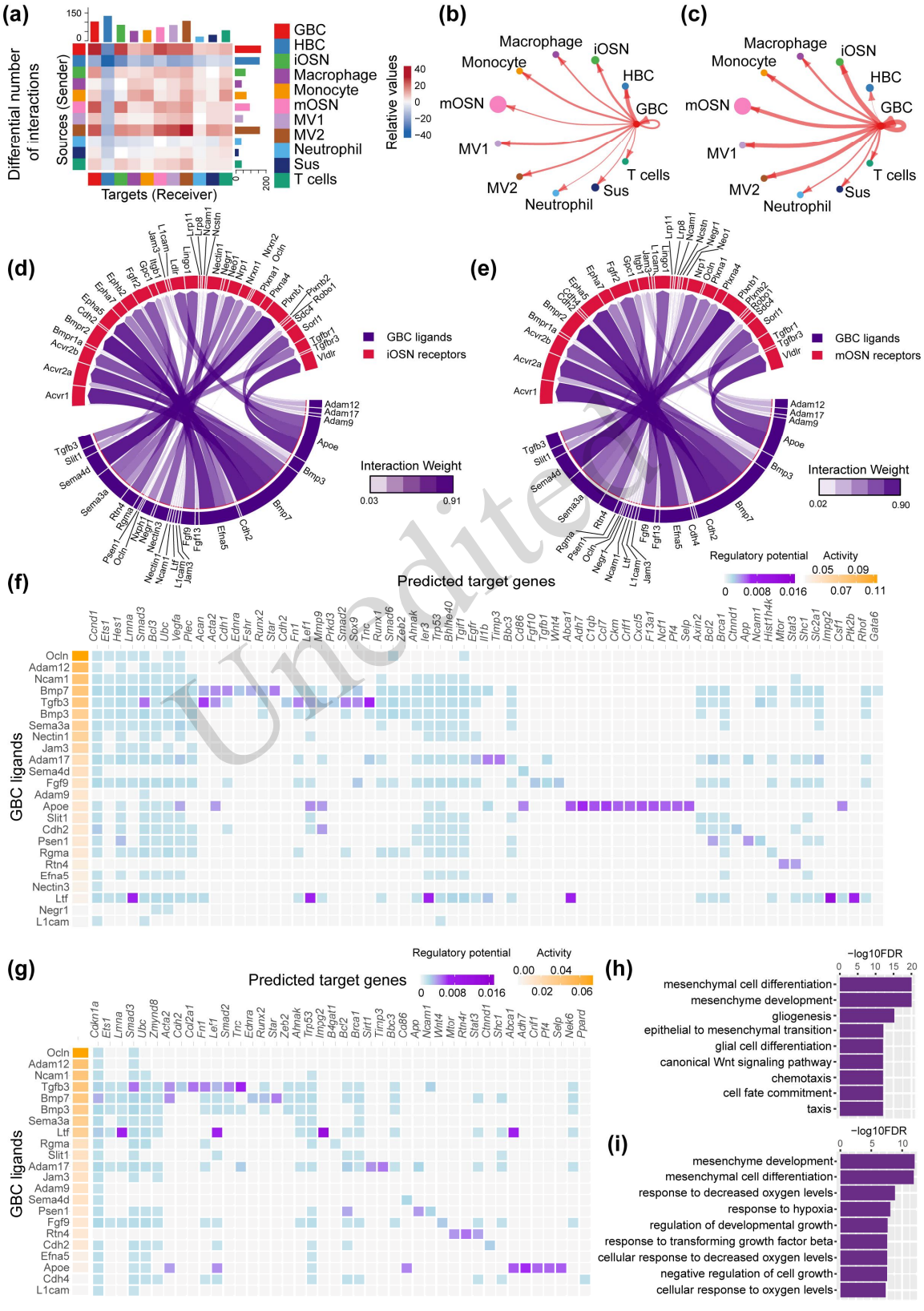

Fig. 3 Tmem59 deficiency increases intercellular communication from GBC to OSN. (a) Heatmap showing changes in

intercellular communications in Tmem59$^{-/-}$ OE cell types compared to WT ones. (b, c) Plots showing communication intensity from GBC to other cell types in WT (b) and Tmem59$^{-/-}$ (c) OE. (d, e) Circle plots of communication intensity from upregulated ligands in Tmem59$^{-/-}$ GBCs to receptors in iOSNs (d) and mOSNs (e). (f, g) Heatmap showing upregulated ligands in Tmem59$^{-/-}$ GBCs and their regulated target genes in iOSNs (f) and mOSNs (g). (h, i) GO terms of target genes in iOSNs (h) and mOSNs (i).

3.4 Tmem59 contributes to autophagy-related neuronal differentiation trajectory

To further explore how Tmem59 deficiency affects the OE, we scored all cell types using various gene sets. The DNA repair score was significantly lower in all Tmem59$^{-/-}$ cell types compared to the WT counterparts (Fig. S3a), while scores for oxidative phosphorylation were significantly decreased in all cell types of Tmem59$^{-/-}$ OE (Fig. S3d). The gene set score for DNA damage response was drastically increased in the majority of Tmem59$^{-/-}$ cell types but decreased in Tmem59$^{-/-}$ HBCs (Fig. S3c). Moreover, the gene set scores for autophagy of mitochondrion and macroautophagy were significantly increased in Tmem59$^{-/-}$ GBC, iOSN and mOSN (Figs. S3e and S3f), suggesting that autophagy is likely associated with OSN differentiation.

Subsequently, we asked whether Tmem59 deficiency affects neuronal differentiation from GBCs. A pseudotime differentiation trajectory was drawn by Monocle3 based on GBC_TA, GBC_INP, iOSNs, and mOSNs from WT and Tmem59$^{-/-}$ OE (Figs. 4a-4c). Molecular marker identification along the differentiation trajectory demonstrated the location of GBCs, iOSNs and mOSNs (Fig. 4d). DEGs along this trajectory were classified into 12 modules based on their expression patterns (Figs. 4e and S4). We found that genes in Module5 were enriched in Tmem59$^{-/-}$ mOSNs, while genes in Module7 were in WT mOSNs (Fig. 4e). Upregulated genes in Tmem59$^{-/-}$ group in Module 5 functioned in Golgi vesicle transport, macroautophagy, and regulation of autophagy, and participated in ubiquitin mediated proteolysis, autophagy and mitophagy pathways (Figs. 4f and 4h), while upregulated genes in Module 7 were associated with cellular respiration, oxidative phosphorylation, and mitochondrial respiratory chain complex, mainly participating in the proteasome pathway (Figs. 4g and 4i). KEGG analysis revealed that upregulated genes in Tmem59$^{-/-}$ mOSNs mainly participated in autophagy and ubiquitin mediated proteolysis, while downregulated genes were related with protein processing in endoplasmic reticulum and proteasome (Figs. 4j and 4k). Genes related with mitochondrial respiratory chain complex assembly were downregulated in Tmem59$^{-/-}$ GBCs, iOSNs and mOSNs, compared to their WT counterparts, while mitophagy-related genes were upregulated in Tmem59$^{-/-}$ GBCs, iOSNs and mOSNs (Figs. 4l and 4m). Immunostaining data confirmed the upregulation of Prkn in the Tmem59$^{-/-}$ OE, with an increase in the ratio of Prkn^{+} cells by 26 $\pm$ 2 folds compared to WT tissue (Figs. 4n and 4o, P<0.001). By comparing upregulated macroautophagy-related genes in Tmem59$^{-/-}$ GBC_TA, GBC_INP, iOSN and mOSN (Figs. 5b-5e), nine overlapped genes were identified, including Ambra1 (a positive regulator of autophagy), Clec16a (negative regulation of mitophagy), Sesn1 (negative regulation of cell growth), etc. (Fig. 5a). Immunochemical analysis revealed that the ratio of Ambra1^{+}/Tuj1^{+} iOSNs was significantly increased by 97 $\pm$ 18% (P<0.001) in Tmem59$^{-/-}$ OE compared to WT controls (Figs. 5f and 5g). Thus, Tmem59 contributes to neuronal differentiation in the OE, potentially affecting autophagy in neuronal lineages from GBCs to immature and mature OSN.

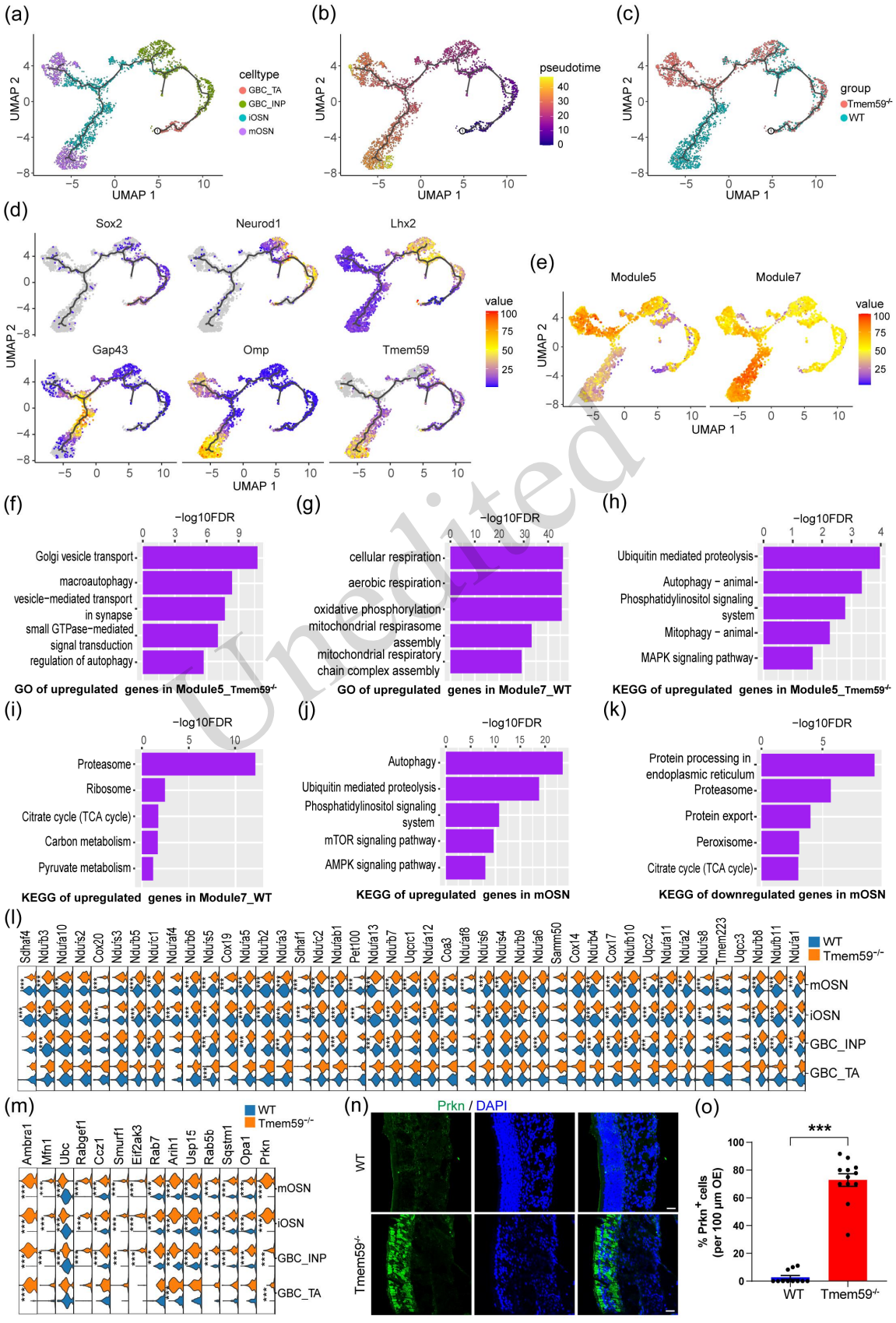
(a)
(b)
(c)
UMAP 2
UMAP 1
celltype
GBC_TA
GBC_INP
iOSN
mOSN
pseudotime
group
Tmem59-/-
WT
(d)
Sox2
Neurod1
Lhx2
Gap43
Omp
Tmem59
value
(e)
Module5
Module7
(f)
−log10FDR
Golgi vesicle transport
macroautophagy
vesicle−mediated transport in synapse
small GTPase−mediated signal transduction
regulation of autophagy
GO of upregulated genes in Module5_Tmem59-/-
(g)
cellular respiration
aerobic respiration
oxidative phosphorylation
mitochondrial respirasome assembly
mitochondrial respiratory chain complex assembly
GO of upregulated genes in Module7_WT
(h)
Ubiquitin mediated proteolysis
Autophagy − animal
Phosphatidylinositol signaling system
Mitophagy − animal
MAPK signaling pathway
KEGG of upregulated genes in Module5_Tmem59-/-
(i)
Proteasome
Ribosome
Citrate cycle (TCA cycle)
Carbon metabolism
Pyruvate metabolism
KEGG of upregulated genes in Module7_WT
(j)
Autophagy
Ubiquitin mediated proteolysis
Phosphatidylinositol signaling system
mTOR signaling pathway
AMPK signaling pathway
KEGG of upregulated genes in mOSN
(k)
Protein processing in endoplasmic reticulum
Proteasome
Protein export
Peroxisome
Citrate cycle (TCA cycle)
KEGG of downregulated genes in mOSN
(l)
WT
Tmem59-/-
mOSN
iOSN
GBC_INP
GBC_TA
(m)
(n)
Prkn / DAPI
WT
Tmem59-/-
(o)
% Prkn+ cells (per 100 μm OE)
***

Fig. 4 Tmem59 deficiency leads to macroautophagy-related changes along the neuronal differentiation trajectory. (a, b) UMAP plots showing the differentiation trajectory from GBC to mOSN. (c) Distribution of WT and Tmem59$^{-/-}$ cells along the neuronal differentiation trajectory. (d) UMAP plots showing the expression of molecular markers for GBC, iOSN and mOSN. (e) Distribution of DEGs in enriched Tmem59$^{-/-}$ and WT mOSNs in Module5 and Module7. (f, g) GO terms of upregulated genes in Module5 (f) and in Module7 (g). (h, i) KEGG analysis on upregulated genes in Module5 (h) and Module7 (i). (j, k) KEGG analysis of upregulated (j) and downregulated (k) genes in Tmem59$^{-/-}$ mOSNs compared to WT counterparts. (l, m) Violin plots showing gene expression related with mitochondrial respiratory chain complex assembly (l) and mitophagy (m) in WT and Tmem59$^{-/-}$ GBC, iOSN and mOSN. (n, o) Confocal images (n) and quantification (o) of Prkn^{+} cells in WT and Tmem59$^{-/-}$ OE. The statistical difference was determined by two-tailed Wilcoxon rank-sum test in (l, m), and unpaired t test in (o). ns, not significant, ***p<0.001. All statistic data were from three mice in each group. Scale bar: 25 μm.

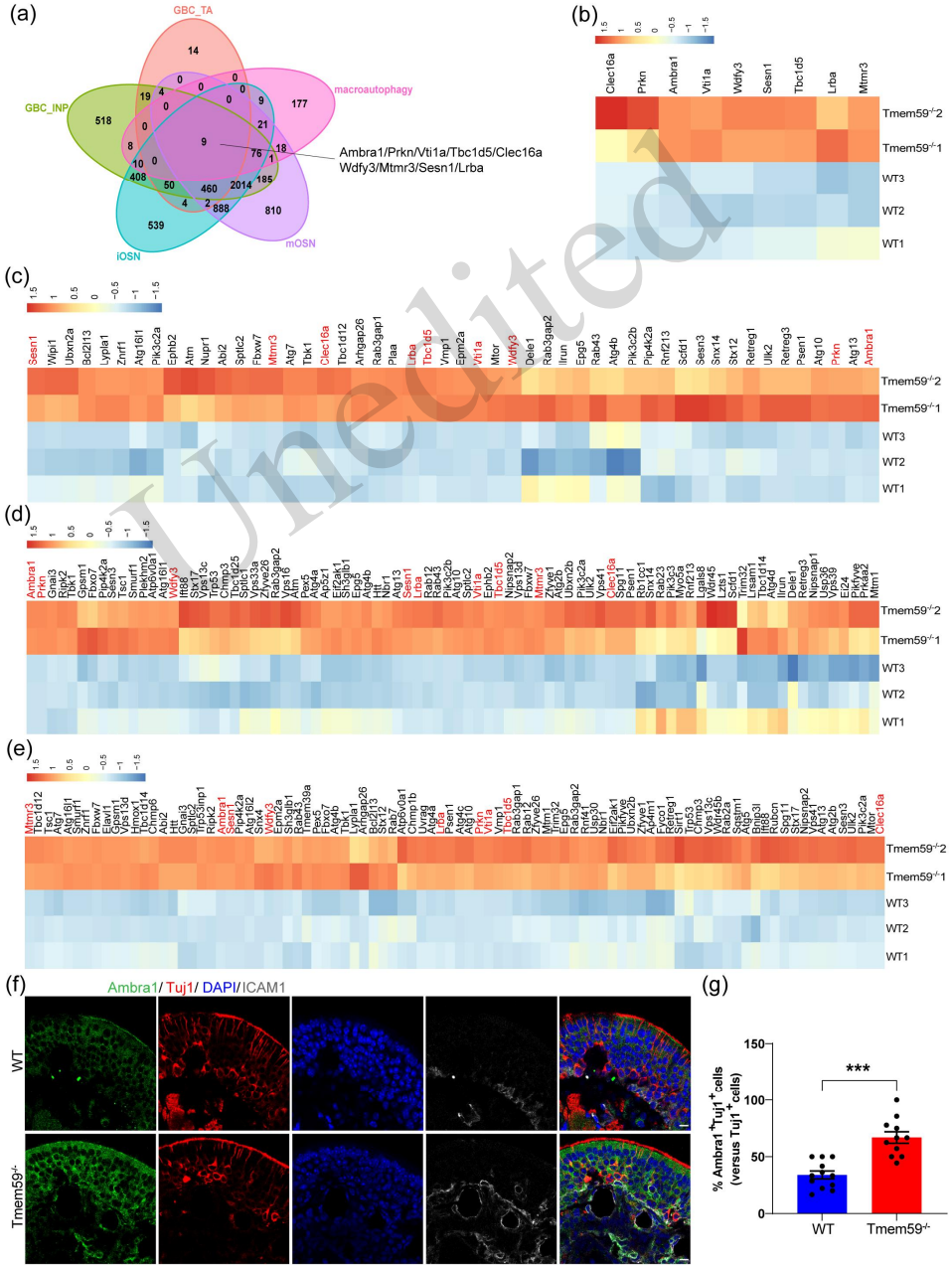

Fig. 5 Upregulation of macroautophagy-related genes in Tmem59$^{-/-}$ GBCs and OSNs. (a) Common

macroautophagy-related genes among GBC, iOSN and mOSN. (b-e) Heatmaps showing expression of macroautophagy-related genes in WT and Tmem59$^{-/-}$ GBC_TA (b), GBC_INP (c), iOSN (d), and mOSN (e). (f) Confocal images of Ambra1^{+} cells in Tuj1^{+} iOSNs from WT and Tmem59$^{-/-}$ OE. (g) Quantification of Ambra1^{+}Tuj1^{+} cells in the WT and Tmem59$^{-/-}$ OE. ***p<0.001. All statistical data were from two mice in each group. Scale bar: 10 μm.

To further investigate if Tmem59 deficiency affects aging-related gene expression in neuronal lineage, we screened DEGs in the GenAge database. Several aging-related genes were differentially expressed in Tmem59$^{-/-}$ sensory neurons, like in Tmem59$^{-/-}$ GBCs, such as the upregulation of Pappa, Mgat5, Insr, Cdk7, Per2, and Igf1r, as well as the downregulation of Gpx4, Cebpb, and Txn1 in either immature and mature OSNs (Fig. S5). Furthermore, Tmem59$^{-/-}$ GBCs also exhibited the differential expression of genes related to nasal diseases including rhinitis and anosmia (Figs. S6a and S6b), and these disease-related genes were also differentially expressed in HBC, iOSN and mOSN (Figs. S6c-S6h). Therefore, Tmem59 deficiency leads to autophagy-related variation in neuronal differentiation trajectory and aging-associated transcriptomic difference in sensory neurons.

Immunostaining data indicated that Tmem59 deletion reduced the ratio of Ki67^{+} cells by 37 ± 5% in the OE (Figs. 6a and 6b, P<0.001), suggesting impaired cell proliferation by Tmem59 deficiency. We also found decreases in the ratio of GAP43^{+} and Pgp9.5^{+} cells by 35 ± 4% and 36 ± 4% in Tmem59$^{-/-}$ OE compared to WT controls (P<0.0001), showing the attenuation of sensory neuronal generation by Tmem59 deficiency (Figs .6c-6f). Moreover, the ratio of cleaved Caspase 3^{+} cells was elevated by 141 ± 36% in Tmem59$^{-/-}$ OE compared to their WT counterparts (Figs. 6g and 6h, P<0.001), indicating that Tmem59 deletion enhances apoptosis in the OE. Collectively, we concluded that Tmem59 deficiency leads to impairments in cell proliferation and neuronal generation, as well as exacerbated cell apoptosis in the OE.

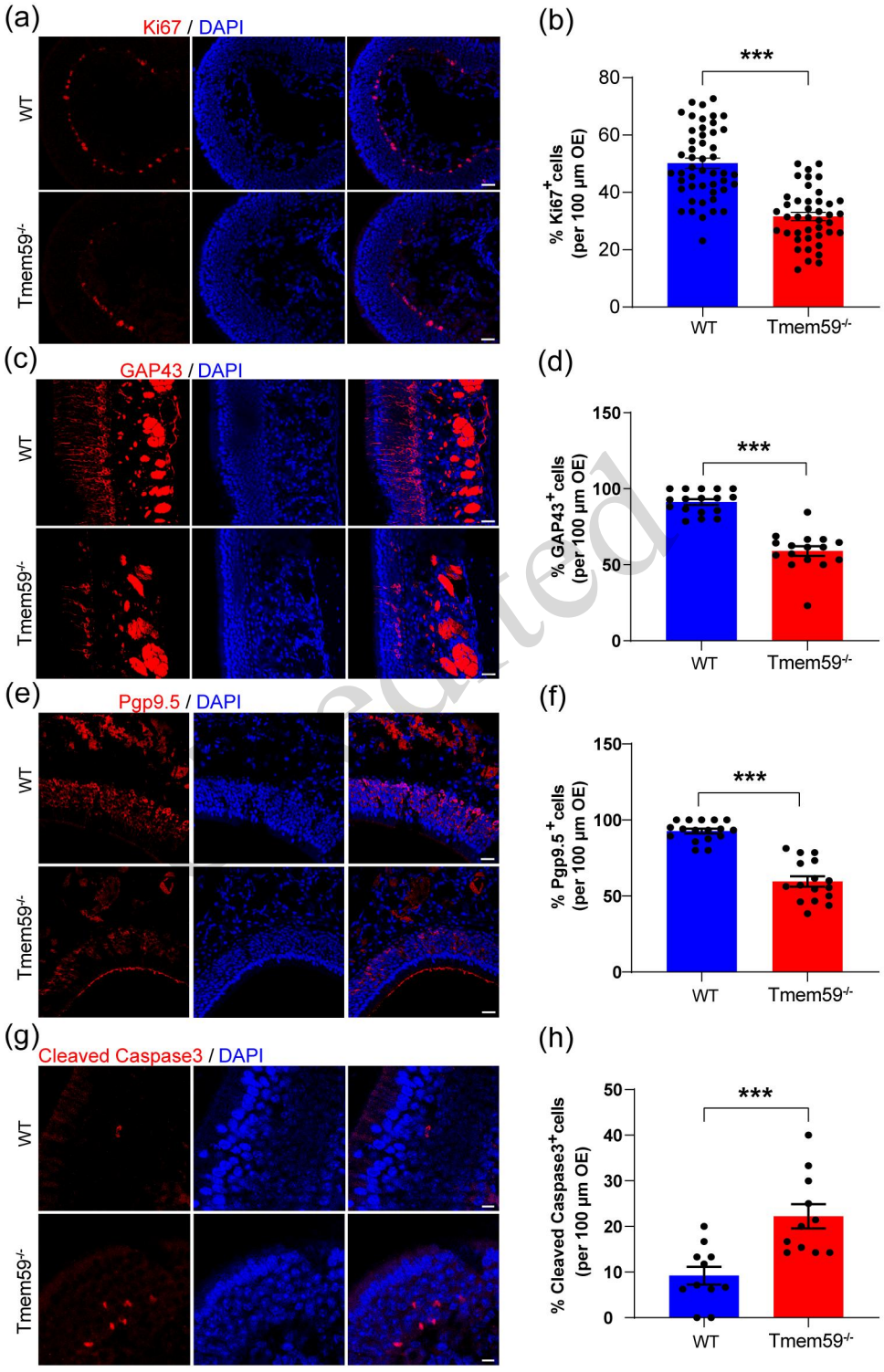

Fig. 6 Tmem59 deficiency impairs cell proliferation and neuronal generation and enhances apoptosis in the OE. Confocal images and quantification of the ratio of Ki67$^+$ (a, b), GAP43$^+$ (c, d), Pgp9.5$^+$ (e, f), and cleaved Caspase 3$^+$ (g, h) cells in the WT and Tmem59$^{-/-}$ OE. The statistical difference was determined by unpaired t test. ***p<0.001. All statistical data were from three mice in each group. Scale bars: 25 μm in (a, c, e), 7.5 μm in (g).

3.5 Transcriptional variation of immune cells in Tmem59$^{-/-}$ OE

Our previous work showed that Tmem59 deletion triggers OE inflammatory activation (Ma, et al., 2023). Here, we identified possible regulators to this inflammatory response. GO analysis revealed that upregulated genes in four types of immune cells including macrophages, monocytes, neutrophils and T cells with Tmem59 deletion functioned in small GTPase-mediated signal transduction and other processes, while downregulated genes were primarily associated with ribosome assembly (Figs. 7a and 7b). SCENIC analysis identified transcriptional hubs in these immune cells, such as Zeb2 in macrophages, Foxp1 in neutrophils, Msi2 in monocytes and T cells (Figs. 7c, 7d, 7g, 7h). KEGG enrichment analysis showed that target genes to Zeb2 in macrophages participated in chemokine signaling pathway and inflammatory mediator regulation, while target genes to Foxp1 in neutrophils were involved in MAPK signaling pathway (Figs. 7c and 7d). Immunochemical data showed that the ratio of Zeb2^{+}/F4/80^{+} macrophages was significantly increased by 96 ± 16% (P<0.001) in Tmem59$^{-/-}$ OE compared to WT ones (Figs. 7e and 7f). Moreover, target genes to Msi2 were correlated with cellular senescence in monocytes and involved in the cGMP-PKG signaling pathway in T cells (Figs. 7g and 7h). Interestingly, these target genes to transcriptional hubs regulate a series of neural processes, such as dendrite development, postsynapse organization, axon guidance, and neuron maturation (Figs.7c, 7d, 7g, 7h), suggesting that these immune cells may regulate activities of sensory neurons. The top significantly upregulated genes by Tmem59 deficiency included Tex14 (functioning in mitotic spindle assembly checkpoint signaling) in all four cell types, and Lrmda [a key regulator of immune homeostasis (Song et al., 2025)] in monocytes and neutrophils. The top downregulated genes contained Rnaset2b, the deficiency of which causes neuroinflammation (Kettwig et al., 2021) in macrophages, monocytes and T cells, and antigen-presentation gene H2-Eb1 in macrophages and monocytes (Fig. 7i). Collectively, in the Tmem59 knockout model, immune cells residing within the OE exhibited transcriptional alterations.

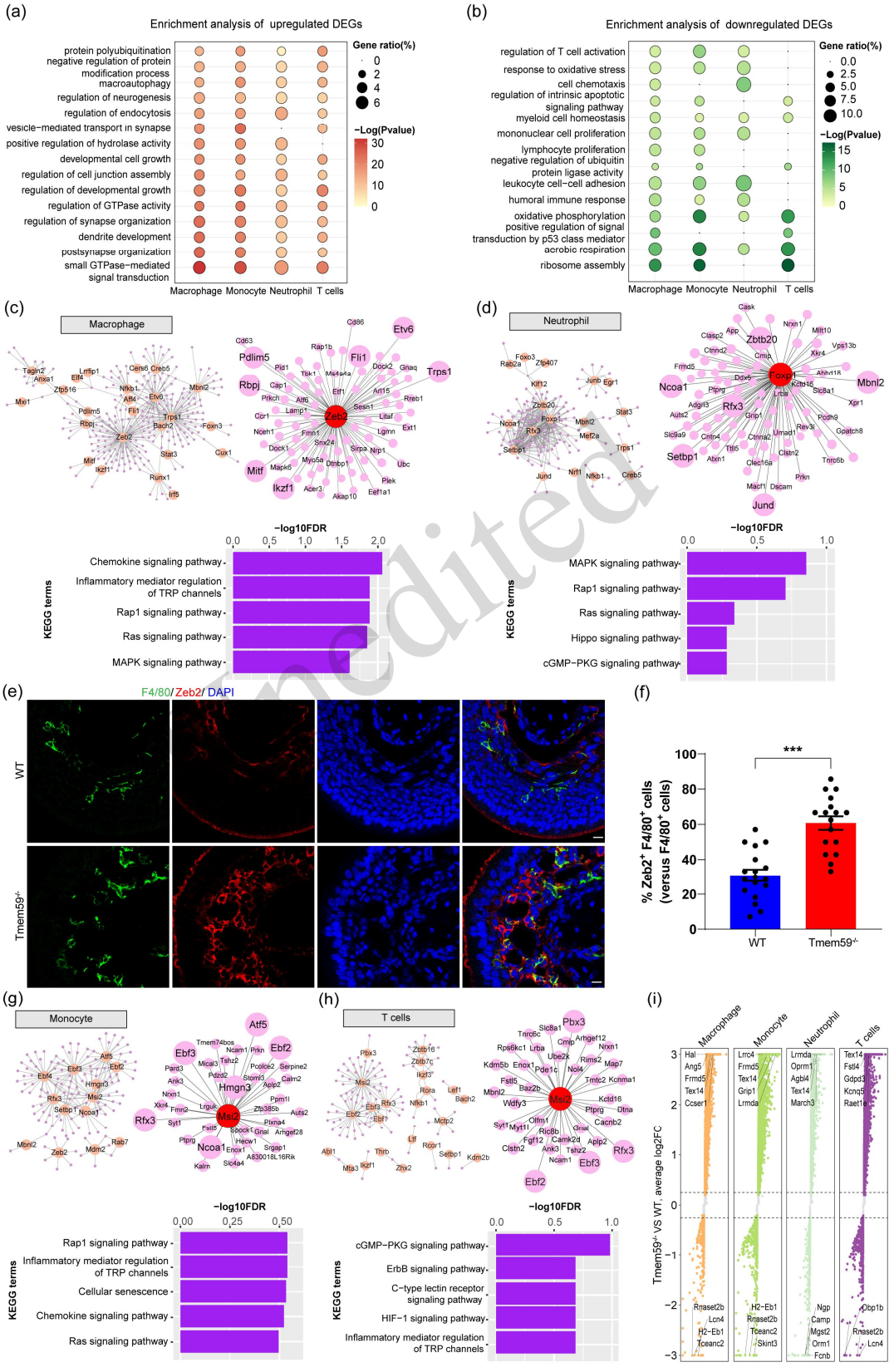

Fig. 7 Transcriptional alterations in Tmem59-deficient immune cells. (a, b) GO terms of upregulated (a) and

downregulated (b) genes in Tmem59$^{-/-}$ macrophages, monocytes, neutrophils, and T cells compared to their WT counterparts. (c, d, g, h) Transcriptional network and representative hub and its target genes (up), as well as GO terms of target genes (bottom) in macrophages (c), neutrophils (d), monocytes (g), and T cells (h). (e) Confocal images of Zeb2^{+} cells in F4/80^{+} macrophages from WT and Tmem59$^{-/-}$ OE. (f) Quantification of Zeb2^{+}/F4/80^{+} cells in the WT and Tmem59$^{-/-}$ OE. (i) Plot showing top 5 upregulated and downregulated genes in Tmem59$^{-/-}$ macrophages, monocytes, neutrophils, and T cells compared to WT counterparts. ***p<0.001. All statistical data were from three mice in each group. Scale bar: 10 μm.

3.6 Tmem59-deficient OE organoids show massive transcriptional alteration

To further explore the functions of Tmem59 in the OE, we established an in vitro OE organoid model. We verified the successful generation and cellular composition of these cultured organoids by immunostaining for typical OE markers, such as OMP, IL33 and ICAM1 (Fig. S7). RNA-Seq analysis was performed on WT and Tmem59$^{-/-}$ OE organoids (Fig. 8a). Tmem59$^{-/-}$ organoids showed apparent transcriptional change when compared to their WT counterparts (Fig. 8b). Several inflammation-related genes were among the top 20 upregulated genes in Tmem59$^{-/-}$ organoids compared to WT controls, including Bpifa1, Cxcl1 and Ccl20. Other highly upregulated genes contained Cdkn2a, a positive regulator of apoptotic process and cell proliferation inhibitor, Ccn2, a reported cellular senescence activator (Tejedor-Santamaria et al., 2025) and DNA damage aggravator (Valentijn et al., 2022), and Lcn2, an inflammatory promoter (Li et al., 2023; Wang et al., 2024) (Fig. 8c). Tmem59 deficiency also caused the downregulation of several critical transcriptional factors in OE organoids, such as Fos, a neuronal activation gene, Cbx6, a regulator of stem cell identity (Santanach et al., 2017), and Zfp36, an inducer to degradation of inflammatory cytokines (Yadav et al., 2024)(Fig. 8d). GO analysis revealed that upregulated genes in Tmem59$^{-/-}$ OE organoids contributed to cilium assembly, leukocyte migration and cell chemotaxis, while downregulated genes were mainly involved in epithelial cell proliferation, extracellular matrix assembly, and antigen processing and presentation (Figs. 8e and 8f). Interestingly, some DEGs in Tmem59$^{-/-}$ organoids were diseased-associated genes (Figs. 8g and 8h), further supporting that Tmem59 deficiency causes the differential expression of nasal disease-related genes in the OE.

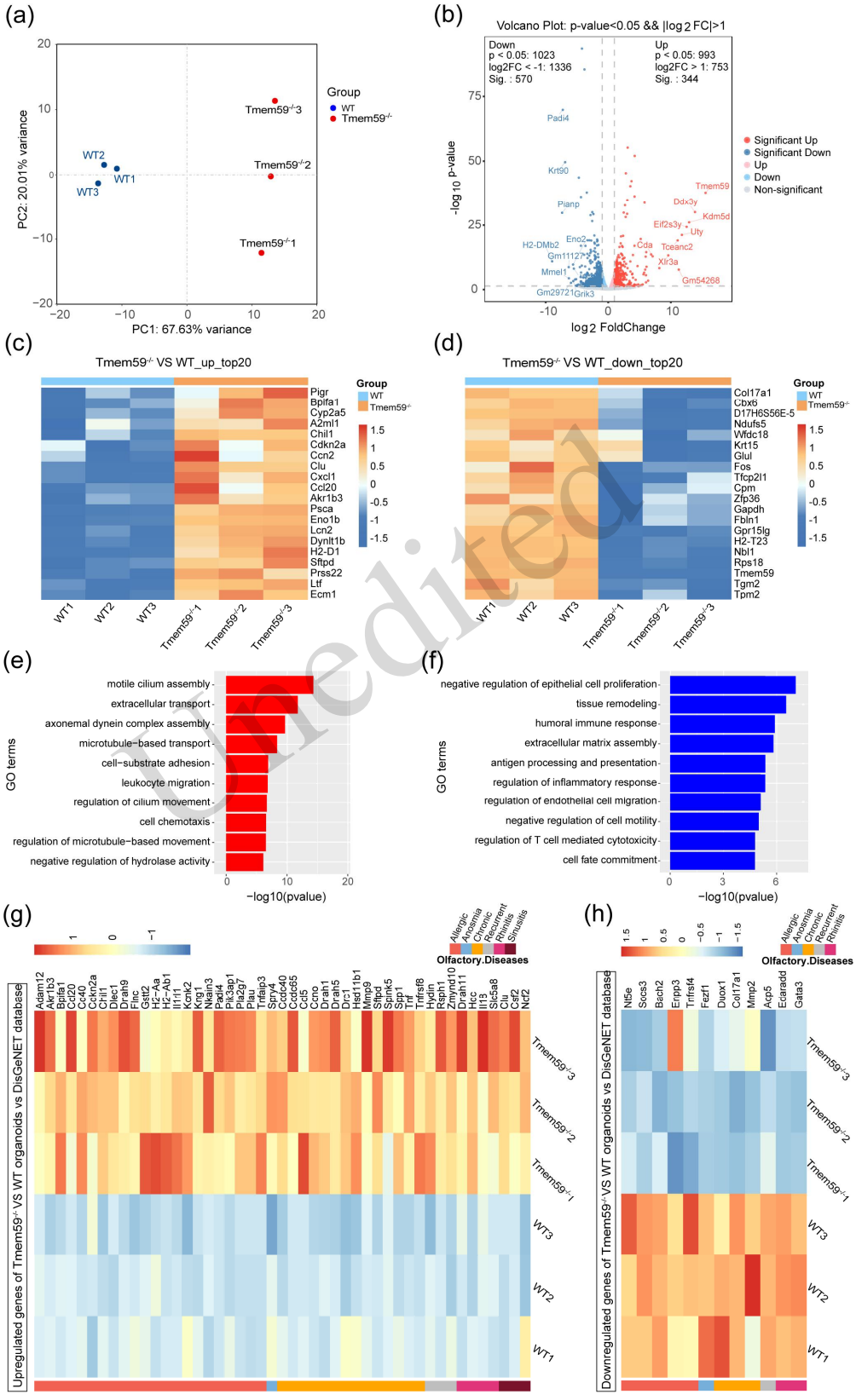

Fig. 8 Transcriptional alteration in Tmem59$^{-/-}$ OE organoids. (a) PC analysis of bulk RNA-Seq data for WT and

Tmem59$^{-/-}$ OE organoid samples. (b) Volcano plot showing upregulated and downregulated genes in Tmem59$^{-/-}$ organoids compared to WT ones. (c, d) The top 20 upregulated (c) and downregulated (d) genes in Tmem59$^{-/-}$ organoids compared to WT ones. (e, f) GO terms of upregulated (e) and downregulated (f) genes in Tmem59$^{-/-}$ organoids compared to WT ones. (g, h) Heatmaps of upregulated (g) and downregulated (h) genes associated with nasal diseases in Tmem59$^{-/-}$ organoids compared to WT ones.

4 Discussion

In this study, we found that Tmem59 deficiency leads to the differential expression of aging- and nasal diseases-related genes in basal cells and sensory neurons. Intercellular communications from GBCs to sensory neurons were promoted by Tmem59 deficiency, potentially affecting neuron apoptosis and cell proliferation. Tmem59 deletion also altered neuronal differentiation trajectory, mediated by macroautophagy-associated processes. Cell proliferation and neuronal generation in the OE was impaired, while apoptosis was enhanced by Tmem59 deficiency. Our *in vitro* cultured organoid model confirmed the massive transcriptional alteration and differential expression of nasal disease-related genes by Tmem59 deletion. Collectively, our comprehensive analysis revealed certain critical roles of Tmem59 in GBC and sensory neurons.

A major finding in the current study is that Tmem59 deficiency leads to the senescent states in basal cells and sensory neurons, with higher scores of senescence gene sets and the differential expression of aging-associated genes (Figs. 2 and S5). Currently, there is no report showing the direct correlation between Tmem59 deletion and senescence. Crucially, these findings must be reconciled with the current understanding of Tmem59 in Alzheimer's disease (AD), which correlates with senescence. Tmem59 regulates multiple aspects of the amyloid precursor protein, including its complex glycosylation, cell surface expression, and secretion (Ullrich et al., 2010). The lack of Tmem59 exerts a neuroprotective effect by reducing toxic amyloid β(Aβ) aggregation, thereby alleviating memory dysfunction in transgenic AD models (Meng et al., 2020; Li et al., 2021). Therefore, Tmem59 inhibition might serve as a therapeutic strategy for amyloid clearance in the central nervous system. While these studies highlight the regulatory role of Tmem59 in Aβ toxicity, Tmem59 deficiency causes a series of events closely associated with aging under non-pathological conditions without amyloid overload. For example, Tmem59 deficiency in microglia impairs synapse engulfment (Meng, et al., 2022), while aging is one of the highest risk factors for microglial phagocytosis (Gabande-Rodriguez et al., 2020). Tmem59 deletion was also reported to induce hypomyelination and impair neurological function (Feng et al., 2021), and hypomyelination was observed with advanced aging (Philips et al., 2026). Our previous work showed that Tmem59 deficiency causes sensory neuronal loss and inflammatory activation in the OE (Ma, et al., 2023), both of which are features in aged OE as increasingly aneuronal areas (Child et al., 2018) and the recruitment and activation of immune cells in aged OE (Wang et al., 2025b). Thus, it is reasonable that Tmem59 deficiency causes senescent states in the OE.

Continuous neuronal turnover occurs to replace damaged sensory neurons in the OE. Our previous study showed the loss of sensory neurons in the OE by Tmem59 deletion (Ma, et al., 2023). In the present study, we found that upregulated genes associated with macroautophagy were enriched in Tmem59$^{-/-}$ mOSNs (Figs. 4 and 5). As a cellular process, macroautophagy captures large cellular cargos and directs them to lysosomes for degradation. Macroautophagy is reported to be upregulated in senescent cells (Carroll et al., 2017). This may explain our findings that macroautophagy-related genes were significantly upregulated in Tmem59$^{-/-}$ GBCs and OSNs (Fig. 4), since Tmem59 deletion promoted senescence. Nine upregulated genes were overlapped among GBC, iOSN and mOSN by screening with the macroautophagy gene set (Fig. 5). Ambra1 participates in proliferation arrest and autophagy control (Akatsuka et al., 2017). It was demonstrated that Ambra1 regulates cyclin D to determine cells to enter the proliferative or the quiescent phase (Maiani et al., 2021). Thus, the upregulation of Ambra1 in Tmem59$^{-/-}$ GBCs may restrain cells into the quiescence and impair cell proliferation. Prkn pathway is a ubiquitin-dependent pathway for mitochondrial autophagy. Excessive upregulation of Prkn may induce abnormal mitophagy and exacerbate inflammation (Tian et al., 2025). Thus, macroautophagy is a

major effector by Tmem59 deletion on neuronal differentiation trajectory, potentially via affecting cell proliferation and inflammation.

Our previous work showed that Tmem59 deletion induced inflammatory activation in the OE (Ma, et al., 2023), Herein, we proposed that this excessive inflammatory response may correlate with abnormal upregulation in macrophagy pathways. Furthermore, we identified differentially expressed transcriptional network hubs in immune cells. Zeb2 was upregulated in macrophages after Tmem59 deletion. A previous study showed that Zeb2 knockdown using in vitro experiments lowered IL-6 and TNF-α levels in macrophages, whereas Zeb2 overexpression aggravated the macrophage-induced inflammation (Zhang et al., 2025). This supports our findings that Tmem59 deficiency-induced inflammatory activation may associate with Zeb2 upregulation in macrophages. Foxp1 is an upregulated hub in Tmem59$^{-/-}$ neutrophils (Fig. 7). It was reported that Foxp1 expression is upregulated in neutrophils treated with inflammatory stimuli (Ismailova et al., 2023). Moreover, inflammatory response was enhanced by M1 macrophage polarization, which was triggered by H3K9me2 methylation within the Foxp1 promoter region (Li et al., 2022). These findings imply that Tmem59 deletion-related Foxp1 upregulation in neutrophils is induced by inflammatory activation in the OE. The other important hub is Msi2 upregulated in T cells with Tmem59 deletion. Msi2 knockdown promoted cell proliferation in kidney renal clear cell carcinoma by regulating T cell function (Yang et al., 2025), hence the upregulation of Msi2 in T cells may contribute to impaired cell proliferation in Tmem59$^{-/-}$ OE. Collectively, the upregulation of transcriptional hubs in immune cells by Tmem59 deletion is responsible for inflammatory activation and proliferative deficits.

5 Conclusions

In summary, this study provides a comprehensive view of transcriptional changes in the OE with Tmem59 deficiency. The Tmem59 knockout-induced senescent state and macroautophagy-related changes along the neuronal differentiation trajectory suggest this gene as a potential target for therapy against olfactory dysfunction.

Data availability statement

The scRNA-Seq datasets of WT and Tmem59$^{-/-}$ OE tissues generated during the current study are available in the China National GeneBank DataBase (CNGBdb) repository (CNP0008897). The dataset and 3D plot of differentially expressed genes in WT and Tmem59$^{-/-}$ OE are available at https://www.olfaging.com/.

Acknowledgments

This work was supported by National Natural Science Foundation of China Grants (No. 82571283 and 32271044), Science and Technology Commission of Shanghai Municipality (No. 23ZR1409600), Open research fund (No. gect-2025-Z06 and gect-2025-Q05) of Shanghai Key Laboratory of Gene Editing and Cell Therapy for Rare Diseases. We acknowledge the Medical Science Data Center of Fudan University for supporting the scRNA-Seq data analysis and thank the staff members of the Integrated Laser Microscopy System at the National Facility for Protein Science in Shanghai (NFPS) for confocal data collection.

Author contributions

Yiqun YU conceived the project. Ping ZHOU and Weihao LI conducted scRNA-Seq bioinformatic analyses. Ping ZHOU performed laboratory experiments. Ping ZHOU and Yiqun YU analyzed the resulting data. Ping ZHOU, Weihao LI, and Yiqun YU prepared figures and wrote the manuscript. Yiqun YU finalized manuscript. All authors have read and approved the final manuscript, and therefore, have full access to all the data in the study and take responsibility for the integrity and security of the data.

Compliance with ethics guidelines

Ping ZHOU, Weihao LI, and Yiqun YU declare that they have no conflicts of interest.

The procedures of animal breeding and tissue harvesting were approved by the Institutional Animal Care and Use Committee in Eye & ENT Hospital, Fudan University (Permit number: IACUC-DWZX-2025-053).

Declaration on the use of generative AI tools

During the preparation of this work, the authors used DeepSeek and Grammarly to improve language and readability, and to check for grammatical errors. After using this tool, the authors reviewed and edited the content as needed and take full responsibility for the content of the publication.

References

Schwob JE, Jang W, Holbrook EH, et al., 2017. Stem and progenitor cells of the mammalian olfactory epithelium: Taking poietic license. *J Comp Neurol*, 525(4):1034-1054. https://doi.org/10.1002/cne.24105

Gadye L, Das D, Sanchez MA, et al., 2017. Injury activates transient olfactory stem cell states with diverse lineage capacities. *Cell Stem Cell*, 21(6):775-790 e779. https://doi.org/10.1016/j.stem.2017.10.014

Li W, Wu T, Zhu K, et al., 2024. A single-cell transcriptomic census of mammalian olfactory epithelium aging. *Dev Cell*, 59(22):3043-3058 e3048. https://doi.org/10.1016/j.devcel.2024.07.020

Wu T, Li W, Zhuang L, et al., 2025. Deficiency of aging-related gene chitinase-like 4 impairs olfactory epithelium homeostasis. *Cell Prolif*, 58(8):e70055. https://doi.org/10.1111/cpr.70055

Ko T, Choi R, Issa K, et al., 2023. Polycomb repressive complex 2 regulates basal cell fate during adult olfactory neurogenesis. *Stem Cell Reports*, 18(11):2283-2296. https://doi.org/10.1016/j.stemcr.2023.09.008

Liu Q, Feng R, Chen Y, et al., 2018. Dcf1 triggers dendritic spine formation and facilitates memory acquisition. *Mol Neurobiol*, 55(1):763-775. https://doi.org/10.1007/s12035-016-0349-6

Meng J, Han L, Zheng N, et al., 2022. Microglial tmem59 deficiency impairs phagocytosis of synapse and leads to autism-like behaviors in mice. *J Neurosci*, 42(25):4958-4979. https://doi.org/10.1523/JNEUROSCI.1644-21.2022

Wang J, Li J, Wang Q, et al., 2018. Dcf1 deficiency attenuates the role of activated microglia during neuroinflammation. *Front Mol Neurosci*, 11:256. https://doi.org/10.3389/fnmol.2018.00256

Zhang L, Wang T, Chen XF, et al., 2021. Tmem59 protects against cerebral ischemic stroke by suppressing pyroptosis and microglial activation. *Biochem Biophys Res Commun*, 543:72-79. https://doi.org/10.1016/j.bbrc.2020.09.013

Ma Z, Li W, Zhuang L, et al., 2023. Tmem59 ablation leads to loss of olfactory sensory neurons and impairs olfactory functions via interaction with inflammation. *Brain Behav Immun*, 111:151-168. https://doi.org/10.1016/j.bbi.2023.04.005

Wang L, Ren W, Li X, et al., 2021. Chitinase-like protein ym2 (chil4) regulates regeneration of the olfactory epithelium via interaction with inflammation. *J Neurosci*, 41(26):5620-5637. https://doi.org/10.1523/JNEUROSCI.1601-20.2021

Ren W, Wang L, Zhang X, et al., 2021. Expansion of murine and human olfactory epithelium/mucosa colonies and generation of mature olfactory sensory neurons under chemically defined conditions. *Theranostics*, 11(2):684-699. https://doi.org/10.7150/thno.46750

Liu J, Qi J, Jiang N, et al., 2026. Olfactory epithelium organoid models identify ddit3 as a potential therapeutic target against inflammation-related olfactory sensory neuronal loss and functional deficit. *Int J Biol Sci*, 22(8):4025-4042. https://doi.org/10.7150/ijbs.129192

Luecken MD, Theis FJ, 2019. Current best practices in single-cell rna-seq analysis: A tutorial. *Mol Syst Biol*, 15(6):e8746. https://doi.org/10.15252/msb.20188746

Wang J, Zhou X, Yu P, et al., 2025a. A transcriptome-based human universal senescence index (husi) robustly predicts cellular senescence under various conditions. *Nat Aging*, 5(6):1159-1175. https://doi.org/10.1038/s43587-025-00886-2

Zhang J, Hao C, Jiang J, et al., 2018. The mechanisms underlying olfactory deficits in apolipoprotein e-deficient mice: Focus on olfactory epithelium and olfactory bulb. *Neurobiol Aging*, 62:20-33. https://doi.org/10.1016/j.neurobiolaging.2017.09.036

Chaker Z, Aid S, Berry H, et al., 2015. Suppression of igf-i signals in neural stem cells enhances neurogenesis and olfactory function during aging. *Aging Cell*, 14(5):847-856. https://doi.org/10.1111/acel.12365

Jia J, Liu H, Sun L, et al., 2024. Thioredoxin-1 protects neurons through inhibiting nlrp1-mediated neuronal pyroptosis in models of alzheimer's disease. *Mol Neurobiol*, 61(11):9723-9734. https://doi.org/10.1007/s12035-024-04341-y

Lane-Donovan C, Herz J, 2017. The apoe receptors vldlr and apoer2 in central nervous system function and disease. *J Lipid Res*, 58(6):1036-1043. https://doi.org/10.1194/jlr.R075507

Lee H, Aylward AJ, Pearse RV, 2nd, et al., 2023. Cell-type-specific regulation of apoe and clu levels in human neurons by the alzheimer's disease risk gene sorl1. *Cell Rep*, 42(8):112994. https://doi.org/10.1016/j.celrep.2023.112994

Shen M, Zhou C, Tian Y, et al., 2023. Effects of semaphorin3a on the growth of sensory and motor neurons. *Exp Cell Res*, 424(2):113506. https://doi.org/10.1016/j.yexcr.2023.113506

Mcdermott JE, Goldblatt D, Paradis S, 2018. Class 4 semaphorins and plexin-b receptors regulate gabaergic and glutamatergic synapse development in the mammalian hippocampus. *Mol Cell Neurosci*, 92:50-66. https://doi.org/10.1016/j.mcn.2018.06.008

Song R, Ngoka C, Singla A, et al., 2025. The rab32-lrmda-retriever complex is a key regulator of intestinal immune homeostasis. *bioRxiv*, https://doi.org/10.1101/2025.07.16.665158

Kettwig M, Ternka K, Wendland K, et al., 2021. Interferon-driven brain phenotype in a mouse model of rnaset2 deficient leukoencephalopathy. *Nat Commun*, 12(1):6530. https://doi.org/10.1038/s41467-021-26880-x

Tejedor-Santamaria L, Marquez-Exposito L, Villacampa A, et al., 2025. Ccn2 activates cellular senescence leading to kidney fibrosis in folic acid-induced experimental nephropathy. *Int J Mol Sci*, 26(9) https://doi.org/10.3390/ijms26094401

Valentijn FA, Knoppert SN, Marquez-Exposito L, et al., 2022. Cellular communication network 2 (connective tissue growth factor) aggravates acute DNA damage and subsequent DNA damage response-senescence-fibrosis following kidney ischemia reperfusion injury. *Kidney Int*, 102(6):1305-1319. https://doi.org/10.1016/j.kint.2022.06.030

Li J, Xu P, Hong Y, et al., 2023. Lipocalin-2-mediated astrocyte pyroptosis promotes neuroinflammatory injury via nlrp3 inflammasome activation in cerebral ischemia/reperfusion injury. *J Neuroinflammation*, 20(1):148. https://doi.org/10.1186/s12974-023-02819-5

Wang X, Zhu Z, Zhang Z, et al., 2024. Astrocyte-derived lipocalin 2 promotes inflammation and scarring after spinal cord injury by activating smad in mice. *Exp Neurol*, 380:114915. https://doi.org/10.1016/j.expneurol.2024.114915

Santanach A, Blanco E, Jiang H, et al., 2017. The polycomb group protein cbx6 is an essential regulator of embryonic stem cell identity. *Nat Commun*, 8(1):1235. https://doi.org/10.1038/s41467-017-01464-w

Yadav S, El Hamra R, Alturki NA, et al., 2024. Regulation of zfp36 by isgf3 and mk2 restricts the expression of inflammatory cytokines during necroptosis stimulation. *Cell Death Dis*, 15(8):574. https://doi.org/10.1038/s41419-024-06964-4

Ullrich S, Munch A, Neumann S, et al., 2010. The novel membrane protein tmem59 modulates complex glycosylation, cell surface expression, and secretion of the amyloid precursor protein. *J Biol Chem*, 285(27):20664-20674. https://doi.org/10.1074/jbc.M109.055608

Meng J, Han L, Zheng N, et al., 2020. Tmem59 haploinsufficiency ameliorates the pathology and cognitive impairment in the 5xfad mouse model of alzheimer's disease. *Front Cell Dev Biol*, 8:596030. https://doi.org/10.3389/fcell.2020.596030

Li WH, Gan LH, Ma FF, et al., 2021. Deletion of dcf1 reduces amyloid-beta aggregation and mitigates memory deficits. *J Alzheimers Dis*, 81(3):1181-1194. https://doi.org/10.3233/JAD-200619

Gabande-Rodriguez E, Keane L, Capasso M, 2020. Microglial phagocytosis in aging and alzheimer's disease. *J Neurosci Res*, 98(2):284-298. https://doi.org/10.1002/jnr.24419

Feng R, Wang J, Luo G, et al., 2021. Dcf1 deficiency induces hypomyelination by activating wnt signaling. *Exp Neurol*, 335:113486. https://doi.org/10.1016/j.expneurol.2020.113486

Philips T, Thompson EG, Spead O, et al., 2026. Astrocyte mct1 expression does not contribute to the axonal degenerative phenotype observed with ubiquitous mct1 depletion. *Glia*, 74(2):e70113. https://doi.org/10.1002/glia.70113

Child KM, Herrick DB, Schwob JE, et al., 2018. The neuroregenerative capacity of olfactory stem cells is not limitless: Implications for aging. *J Neurosci*, 38(31):6806-6824. https://doi.org/10.1523/JNEUROSCI.3261-17.2018

Wang S, Cha X, Xie Y, et al., 2025b. Il-17a induces age-related olfactory dysfunction by impairing regeneration and promoting respiratory metaplasia in mice. *Nat Commun*, 17(1):1036. https://doi.org/10.1038/s41467-025-67786-2

Carroll B, Nelson G, Rabanal-Ruiz Y, et al., 2017. Persistent mtorc1 signaling in cell senescence results from defects in amino acid and growth factor sensing. *J Cell Biol*, 216(7):1949-1957. https://doi.org/10.1083/jcb.201610113

Akatsuka H, Kuga S, Masuhara K, et al., 2017. Ambra1 is involved in t cell receptor-mediated metabolic reprogramming through an atg7-independent pathway. *Biochem Biophys Res Commun*, 491(4):1098-1104.

https://doi.org/10.1016/j.bbrc.2017.08.019
Maiani E, Milletti G, Nazio F, et al., 2021. Ambra1 regulates cyclin d to guard s-phase entry and genomic integrity. *Nature*, 592(7856):799-803. https://doi.org/10.1038/s41586-021-03422-5
Tian S, Zhang Y, Liu C, et al., 2025. Double-edged mitophagy: Balancing inflammation and resolution in lung disease. *Clin Sci (Lond)*, 139(19):1047-1072. https://doi.org/10.1042/CS20256705
Zhang MY, Zhang B, Tao QQ, et al., 2025. Single-cell rna sequencing identifies a unique zeb2-regulated clec4d(+) macrophage state contributing to early inflammatory injury in cardiac hypertrophy. *Eur J Pharmacol*, 1002:177867. https://doi.org/10.1016/j.ejphar.2025.177867
Ismailova A, Salehi-Tabar R, Dimitrov V, et al., 2023. Identification of a forkhead box protein transcriptional network induced in human neutrophils in response to inflammatory stimuli. *Front Immunol*, 14:1123344. https://doi.org/10.3389/fimmu.2023.1123344
Li Y, Li G, Zhang L, et al., 2022. G9a promotes inflammation in streptococcus pneumoniae induced pneumonia mice by stimulating m1 macrophage polarization and h3k9me2 methylation in foxp1 promoter region. *Ann Transl Med*, 10(10):583. https://doi.org/10.21037/atm-22-1884
Yang S, Zhang X, Chen X, et al., 2025. Msi2 exerts antitumor effects by regulating t-cell function in kidney renal clear cell carcinoma. *Transl Androl Urol*, 14(11):3664-3684. https://doi.org/10.21037/tau-2025-437

Supplementary information

Figs. S1-S7; Materials and methods